Cithe this as: M. Chen et al. / Polyhedron 113 (2016) 132–143

Access paper at: http://dx.doi.org/10.1016/j.poly.2016.04.015

Six lanthanide supramolecular frameworks based on mixed *m*-/*p*-hydroxybenzoic acid and 1,10-phenanthroline tectons: Syntheses, crystal structures, and properties

Min Chen [a], Min Hu [a], Wen-Ming Xu [a], E. Carolina Sañudo [b], Shao-Ming Fang [a], Chun-Sen Liu [a,⇑]

[a] *Zhengzhou University of Light Industry, Henan Provincial Key Lab of Surface & Interface Science, Zhengzhou, Henan 450002, China*
[b] *Departament de Química Inorgànica i Institut de Nanociència i Nanotecnologia, Universitat de Barcelona, Diagonal, 645, 08028 Barcelona, Spain*

a r t i c l e i n f o

Article history:
Received 6 March 2016
Accepted 12 April 2016
Available online 20 April 2016

Keywords:
Lanthanide supramolecular frameworks
Position isomers
Crystal structure
Magnetic properties
Luminescent properties

a b s t r a c t

To further explore the research of the coordination possibilities of lanthanide ions with *m*-/*p*-hydroxybenzoic acid isomers in the presence of chelating N-donor ligand 1,10-phenanthroline (phen), six lanthanide supramolecular frameworks based on 3- and 4-hydroxybenzoic acids, namely [Dy(*m*-L)(*m*-HL)(phen)]·H_2O (1) (*m*-H_2L = 3-hydroxybenzoic acid), [Ln(*m*-HL)$_3$(phen)] (Ln = Gd for 2 and Tb for 3), [Ln(*p*-HL)$_3$(phen)(H_2O)] (Ln = Dy for 4, Gd for 5, and Tb for 6; *p*-H_2L = 4-hydroxybenzoic acid), were synthesized and characterized. Structural analyses reveal that complex 1 has a two-dimensional (2-D) sheet structure while complexes 2 and 3 take the dinuclear structures in the 3-hydroxybenzoate derivatives. In the 4-hydroxybenzoate derivatives, complexes 4–6 are isostructural and incorporated by monomeric units. Finally, all the complexes exhibit three-dimensional (3-D) supramolecular frameworks (bcu net for 1; bct nets for 2, and 4–6; hex net for 3) with the aid of abundant hydrogen bonding, π···π and C–H···π interactions. The results reveal that the different positions of the –OH substituent and coordination modes of hydroxybenzoic acids adjust the final coordination networks. Moreover, the magnetic and luminescent properties of the complexes have also been investigated and discussed.

1. Introduction

The synthesis of coordination complexes are becoming one of the most active topics due to their various potential magnetic, sorption, catalytic, electric, and fluorescent applications [1–5]. The main building bricks used for the construction of coordination complexes are organic ligands, metal ions, counter ions, and solvent molecules [6]. Among them, the organic ligands act as bridging organic groups between the metal ions, which may differ from each other in their charges (neutral or anionic) [7,8], shapes (rigid or not) [9,10], lengths [11], positions of functional groups [12] and so on. In our preliminary work, we investigated the coordination possibilities of lanthanide ions (Dy^{III} and Gd^{III}) with 2-hydroxybenzoic acid (*o*-H_2L) and 1,10-phenanthroline (phen) [13]. To further explore this research and evaluate the influence of positional isomeric effect on the formation of the coordination complexes, we chose the position isomers of 2-hydroxybenzoic acid, 3- and 4-hydroxybenzoic acids (*m*-H_2L and *p*-H_2L), as the organic ligands in this work. On one hand, the hydroxybenzoic acids (*o*-H_2L, *m*-H_2L, and *p*-H_2L) are good candidates for the construction of coordination networks based on the following considerations: (i) the carboxylate group may exhibit diverse coordination modes; (ii) the hydroxyl group may provide the additional binding site to connect metal atoms; (iii) the carboxylate and hydroxyl groups are good candidates for hydrogen bonds to construct supramolecular structures with higher dimensionality. Furthermore, these three polycarboxylate ligands are closely related and only differentiated by the positions of the –OH substituent, which may afford different supramolecular assemblies in view of their isomeric effect. On the other hand, the introduction of 1,10-phenanthroline (phen) as auxiliary co-ligand into the metal–carboxylate reaction systems will lead to the formation of abundant π·π stacking and C–H·π interactions. In fact, besides coordination bonding, weak intra- or intermolecular interactions are powerful secondary interactions that can further connect low dimensional motifs into higher-dimensional supramolecular frameworks. In these contribution, we herein reported six new lanthanoid(III) coordination complexes based on mixed 3- or 4-hydroxybenzoic acid and phen co-ligand. The effect of positional isomerism on the supramolecular structures, the magnetic, and luminescence properties of the complexes have been investigated and discussed in detail.

⇑ Corresponding author. Fax: +86 371 86609669.
E-mail address: chunsenliu@zzuli.edu.cn (C.-S. Liu).

Table 1
Crystallographic data and structure refinement summary for complexes 1–6.

Complexes reference	1	2	3	4	5	6
Chemical formula	$C_{26}H_{19}N_2O_7Dy$	$C_{66}H_{46}N_4O_{18}Gd_2$	$C_{66}H_{46}N_4O_{18}Tb_2$	$C_{33}H_{25}N_2O_{10}Dy$	$C_{33}H_{25}N_2O_{10}Gd$	$C_{33}H_{25}N_2O_{10}Tb$
Formula weight	633.93	1497.57	1500.91	772.05	766.80	768.47
Crystal system	monoclinic	monoclinic	monoclinic	monoclinic	monoclinic	monoclinic
Space group	$P2_1/c$	$P2_1/c$	$P2_1/c$	$P2_1/c$	$P2_1/c$	$P2_1/c$
a (Å)	11.9829(7)	14.2648(2)	14.2874(2)	12.7726(5)	12.7907(2)	12.7941(4)
b (Å)	15.8574(10)	12.6555(2)	11.76480(18)	12.0546(4)	12.0822(2)	12.0812(2)
c (Å)	12.8148(6)	20.2106(4)	17.5713(3)	20.7515(11)	20.8110(5)	20.7989(8)
a (°)	90.00	90.00	90.00	90.00	90.00	90.00
b (°)	105.911(6)	126.9510(10)	99.5231(15)	110.756(4)	110.675(2)	110.704(3)
c (°)	90.00	90.00	90.00	90.00	90.00	90.00
Unit cell volume (Å^3)	2341.7(2)	2915.76(8)	2912.83(8)	2987.7(2)	3009.00(10)	3007.23(16)
No. of formula units per unit cell (Z)	4	2	2	4	4	4
D_{calc} (g cm^{-3})	1.798	1.706	1.711	1.716	1.693	1.697
Absorption coefficient (mm^{-1})	3.242	2.336	2.489	2.565	2.268	2.415
$F(000)$	1244	1484	1488	1532	1524	1528
R_{int}	0.0286	0.0274	0.0245	0.0315	0.0284	0.0309
Final R_1[a] values ($I > 2\sigma(I)$)	0.0220	0.0251	0.0198	0.0267	0.0264	0.0257
Final wR^2[b] (F^2) values ($I > 2\sigma(I)$)	0.0284	0.0410	0.0448	0.0310	0.0301	0.0289
Goodness of fit (GOF) on F^2	0.971	0.837	1.043	0.744	0.946	0.873

[a] $R_1 = \sum||F_o| - |F_c|| / \sum|F_o|$.
[b] $wR_2 = [\sum w(|F_o|^2 - |F_c|^2)^2 / \sum w(F_o)^2]^{1/2}$, where $w = 1/[\sigma^2(F^2) + (aP)^2 + bP]$. $P = (F^2 + 2F^2)/3$.

2. Experimental

2.1. General information and materials

All the starting reagents and solvents for synthesis were commercially available and used as received without further purification. Elemental analyses (C, H, and N) were performed on a Vario EL III Elementary analyzer. IR spectra were recorded in the range of 4000–400 cm^{-1} on a Tensor 27 OPUS (Bruker) FT-IR spectrome- ter with KBr pellets. The powder X-ray diffraction (XRPD) patterns of 1–6 were recorded on a Bruker D8 Advance diffractometer (Cu Kα, k = 1.54056 Å) at 40 kV and 30 mA, by using a Cu-target tube and a graphite monochromator. The powder samples were prepared by crushing the crystals and the intensity data were recorded by continuous scan in a $2\theta/\theta$ mode from 3° to 80° with a step size of 0.02° and a scan speed of 8° min^{-1}. Simulation of the XRPD spectra was carried out by the single-crystal data and diffraction-crystal module of the MERCURY (*Hg*) program available free of charge via the Internet at http://www.iucr.org. Magnetic measurements were carried out in the Unitat de Mesures Magnètiques (Universitat de Barcelona) on polycrystalline samples (*circa* 30 mg) with a Quantum Design SQUID MPMS-XL magnetometer equipped with a 5 T magnet. Diamagnetic corrections were calculated using Pascal's constants and an experimental correction for the sample holder was applied. The emission/excitation spectra were recorded on an F-7000 (HITACHI) spectrophotometer at room temperature.

2.2. Synthesis of complexes

2.2.1. [Dy(m-L)(m-HL)(phen)]·H_2O (1) and [Ln(m-HL)$_3$(phen)] (Ln = Gd for 2 and Tb for 3)

A mixture of Ln_2O_3 (Dy_2O_3: 0.05 mmol, 18.7 mg for 1; Gd_2O_3: 0.05 mmol, 18.1 mg for 2; Tb_4O_7: 0.025 mmol, 18.7 mg for 3), phen (9.0 mg, 0.05 mmol) and 3-hydroxybenzoic acid (13.8 mg, 0.1 mmol) in H_2O (8 mL) was sealed in a 15 mL Teflon-lined stainless steel container, which was heated at 170 °C for 3 days, and then cooled to room temperature. After washed by water, ethanol, and ether, the block crystals of 1–3 which are suitable for X-ray structure analysis can be further separated successfully under a microscope manually. For 1: Yield: ~30% based on Dy. *Anal.* Calc. for $C_{26}H_{19}N_2O_7Dy$: C, 49.26; H, 3.02; N, 4.42. Found: C, 49.35; H, 2.94; N, 4.50%. IR (KBr pellet, cm^{-1}): 3261m (br), 1596m, 1565s, 1534m, 1434s, 1395s, 1303w, 1269m, 1143w, 1105w, 999w, 968w, 940w, 897w, 865w, 826m, 771m, 727m, 687w, 425w. For 2: Yield: ~30% based on Gd. *Anal.* Calc. for $C_{66}H_{46}N_4O_{18}Gd_2$: C, 52.93; H, 3.10; N, 3.74. Found: C, 52.87; H, 3.15; N, 3.80%. IR (KBr pellet, cm^{-1}): 3261m (br), 1564s, 1532m, 1434s, 1395s, 1345m, 1302m, 1251m, 1104w, 999w, 941w, 897w, 844m, 825m, 770m, 727m, 687w, 420w. For 3: Yield: ~40% based on Tb. *Anal.* Calc. for $C_{66}H_{46}N_4O_{18}Tb_2$: C, 52.81; H, 3.09; N, 3.73. Found: C, 52.87; H, 3.15; N, 3.66%. IR (KBr pellet, cm^{-1}): 3383m (br), 1576m, 1526s, 1406vs, 1343w, 1303w, 1228m, 1106w, 998w, 938w, 893w, 843w, 816w, 770m, 726m, 684w, 425w.

2.2.2. [Ln(p-HL)$_3$(phen)(H_2O)] (Ln = Dy for 4, Gd for 5 and Tb for 6)

The synthesis methods of 4–6 are similar to that for 1–3 except for the use of 4-hydroxybenzoic acid (13.8 mg, 0.1 mmol) instead of 3-hydroxybenzoic acid (13.8 mg, 0.1 mmol). After washed by water, ethanol, and ether, the block crystals of 4–6 which are suitable for X-ray structure analysis can be further separated successfully under a microscope manually. For 4: Yield: ~40% based on Dy. *Anal.* Calc. for $C_{33}H_{25}N_2O_{10}Dy$: C, 51.34; H, 3.26; N, 3.63. Found: C, 51.29; H, 3.22; N, 3.67%. IR (KBr pellet, cm^{-1}): 3235m (br), 1605m, 1543m, 1502m, 1419s, 1391s, 1345m, 1284m, 1219m, 1166m, 1142w, 1101w, 864m, 842m, 792m, 768w, 726m, 707w, 627m, 554w, 508w. For 5: Yield: ~30% based on Gd. *Anal.* Calc. for $C_{33}H_{25}N_2O_{10}Gd$: C, 51.69; H, 3.29; N, 3.65. Found: C, 51.63; H, 3.36; N, 3.69%. IR (KBr pellet, cm^{-1}): 3239m (br), 1605m, 1543m, 1501m, 1417s, 1391s, 1345m, 1286m, 1221m, 1166m, 1141w, 1102w, 864m, 842m, 792m, 768w, 727m, 707w, 629m, 554w, 509w, 419w. For 6: Yield: 40% based on Tb. *Anal.* Calc. for $C_{33}H_{25}N_2O_{10}Tb$: C, 51.58; H, 3.28; N, 3.65. Found: C, 51.64; H, 3.22; N, 3.60%. IR (KBr pellet, cm^{-1}): 3228m (br), 1606s, 1541s, 1501m, 1418vs, 1390vs, 1345w, 1286m, 1219m, 1165m, 1142w, 1103w, 863m, 841w, 790m, 727m, 706w, 632m, 554w, 417w.

2.3. X–ray crystallographic study

Diffraction intensities for complexes 1–6 were collected on Oxford Xcalibur Eos diffractometer with graphite-monochromated Mo Kα radiation (k = 0.71073 Å) at 294(2) K. Multi-scan absorption corrections were performed with the *CrysAlisPro* program [14]. Empirical absorption corrections were carried out using spherical harmonics, implemented in *SCALE3 ABSPACK* scaling algorithm. The structures were solved by direct methods, and all

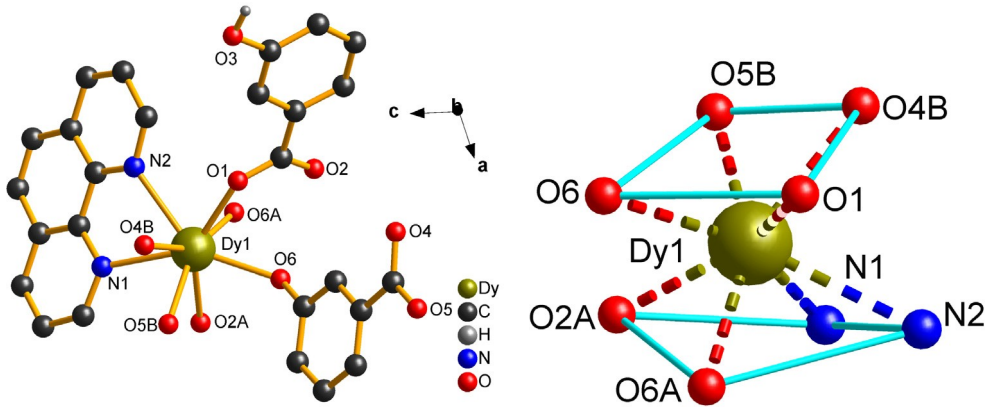

(a)

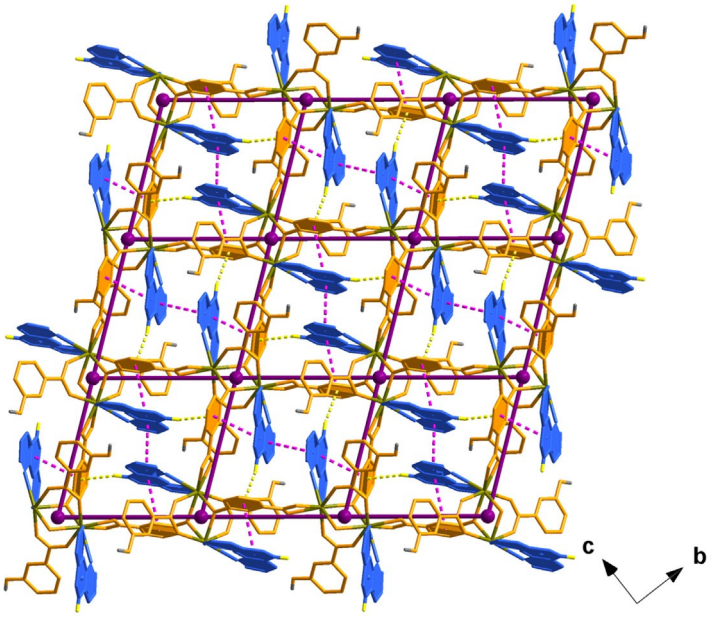

(b)

Fig. 1. (a) View of the local coordination environment (left) and coordination polyhedron (right) of Dy(III) ion in 1. The atoms labeled with the suffixes A and B are generated by the symmetry operations (−x + 2, −y, −z + 1) and (x, −y + 1/2, z + 1/2). (b) View of the (4,4) 2-D sql coordination array with the p···p (pink dashed lines) and C–H···p (yellow dashed lines) interactions. (c) View of the 3-D supramoleuclar framework formed by O–H···O hydrogen-bonding interactions (red dashed lines) around lattice water molecules between adjacent layers with the different 2-D arrays shown in blue and orange colors (left) and a local view of the O–H···O hydrogen-bonding interactions (right). (d) Schematic view of the 3-D bcu net, in which the coordinated bonds and supramolecular interactions are depicted as purple solid and yellow dashed lines, respectively. (Color online.)

non-hydrogen atoms were refined anisotropically on F^2 by the full-matrix least-squares technique using the SHELXTL crystallographic software package [15]. The hydrogen atoms were generated theoretically and refined with isotropic thermal parameters riding on the parent atoms. The details of the crystal parameters, data collection, and refinements for the complexes are summarized in Table 1, and selected bond lengths and angles are listed in Table S1.

3. Results and discussion

3.1. Synthesis

Complexes 1–6 were prepared by assemblies of 3- or 4-hydroxybenzoic acid, 1,10-phenanthroline, and different rare earth oxide as the metal sources under hydrothermal conditions. Complexes 3 and 6 have the metal/acid/phen ratio of 0.5:2:1, while other complexes have the metal/acid/phen ratio of 1:2:1. In the synthetic cases of these complexes, no target products were found under lower reaction temperatures or shorter reaction times. After several attempts, the hydrothermal reaction conditions were intended to be heated at 170 °C for 3 days. For the preparation of all complexes, the crystals of complexes always mixed with a mass of insignificant precipitation. Thus, the bulk synthesized materials were obtained after washed by water, ethanol, and ether. Furthermore, the crystals of all complexes which are suitable for X-ray structure analysis should be further separated under a microscope manually.

3.2. Structure descriptions

3.2.1. Crystal structure of [Dy(m-L)(m-HL)(phen)]·H_2O (1)

Single-crystal X-ray diffraction reveals that 1 has a 2-D coordination array, which is further connected by hydrogen-bonding

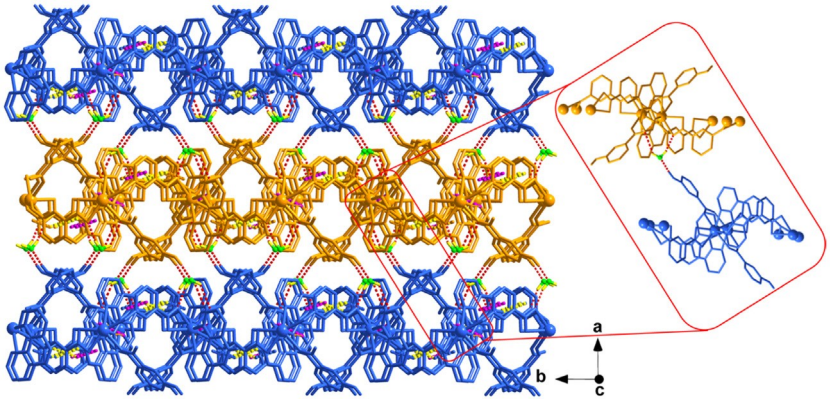

(c)

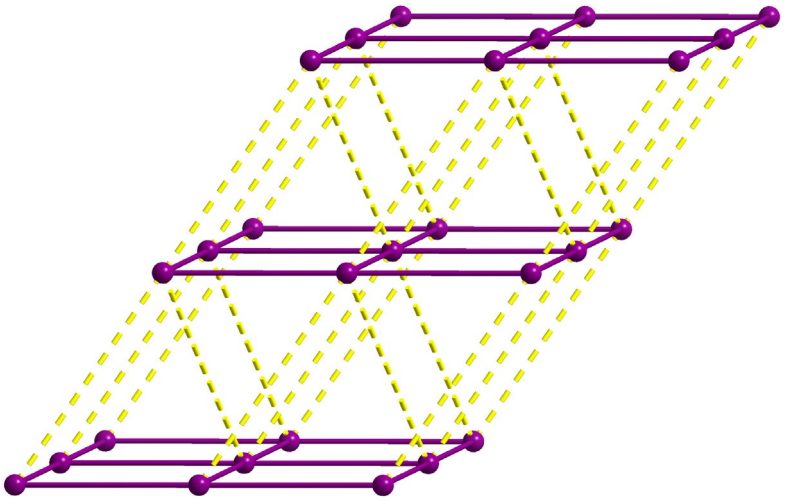

(d)

Fig. 1 (*continued*)

interactions to form a 3-D supramolecular bcu network. The asymmetric unit of 1 contains one Dy(III) ion, one phen, one *m*-L, one *m*-HL ligands, one coordinated and one lattice water molecules. The central Dy(III) ion is eight-coordinated by two hydroxyl oxygen atoms from two different *m*-L ligands, four carboxylate oxygen atoms from three distinct *m*-HL ligands and two nitrogen atoms from two phen ligands to form a distorted square antiprismatic coordination geometry [16] (Fig. 1a). In 1, the *m*-H_2L ligands are partially (only the carboxylate group is deprotonated) and fully deprotonated (both the carboxylate and hydroxyl groups are deprotonated) to take the *m*-HL and *m*-L forms, respectively. The *m*-HL ligand links two Dy(III) ions (Scheme 1a) through the μ_2-η^1:η^1 carboxylate group. The *m*-L ligand shows the μ_3-bridging mode (Scheme 1b) through the μ_1-η^1:η^1 carboxylate group and μ_2-bridging hydroxyl group. The Dy(III) ions are connected by the linkage of *m*-HL and *m*-L ligands to form a 2-D coordination layer (Fig. 1b). The neighboring Dy(III) ions which are bridged by two μ_2-η^1:η^1 carboxylate groups and two μ_2-bridging hydroxyl groups can be regarded as the isolated node with a Dy···Dy distance of 3.6 Å. Thus, the 2-D coordination layer is simplified as an sql (square lattice) layer [17,18]. In addition, the π···π and C–H···π interactions are found in the 2-D sheet. The face-to-face π···π interactions between the neighboring phenanthrolinic and benzenic rings are characterized by the dihedral angle of 7.9° and the centroid···centroid distance of 3.6 Å, while those between the adjacent parallel phenanthrolinic rings are characterized by the dihedral angle of 0.0° and the centroid···centroid distance of 3.6 Å (Table S2) [19]. The C–H···π interactions between the C19–H19A of phen ligand and adjacent benzenic rings (C9–C10–C11–C12–C13–C14) from *m*-L ligand are characterized by the H···Cg separation of 2.70 Å and C–H···Cg angle of 157°, respectively (Cg, the centroid of the ring) (Table S2) [19]. Furthermore, the adjacent parallel 2-D coordination layers are linked by hydrogen-bonding interactions involving the lattice water molecules to form a 3-D supramolecular structure (Fig. 1c) (O3–H3···O7; O7–H7W···O5^i: $i = x-1, y, z$; O7–H8W···O2^i: $i = -x + 1, y + 1/2, -z + 1/2$; see Table S3 for the details) [19]. From the topological view, each dinuclear unit connects other eight ones via both coordination linkages and weak interactions. Thus, the structure of 1 can be described as an 8-connected 3-D non-interpenetrating network with the Point (Schläfli) symbol ($4^{24}\cdot6^4$) calculated by TOPOS program (Fig. 1d) [20], which corresponds to a bcu (body-centered cubic lattice net) topology [17,21].

3.2.2. Crystal structure of [Gd(m-HL)$_3$(phen)] (2)

X-ray crystallographic study reveals that the structure of 2 is made up of neutral centrosymmetric dinuclear units which are further linked through hydrogen-bonding, π···π, and C–H···π

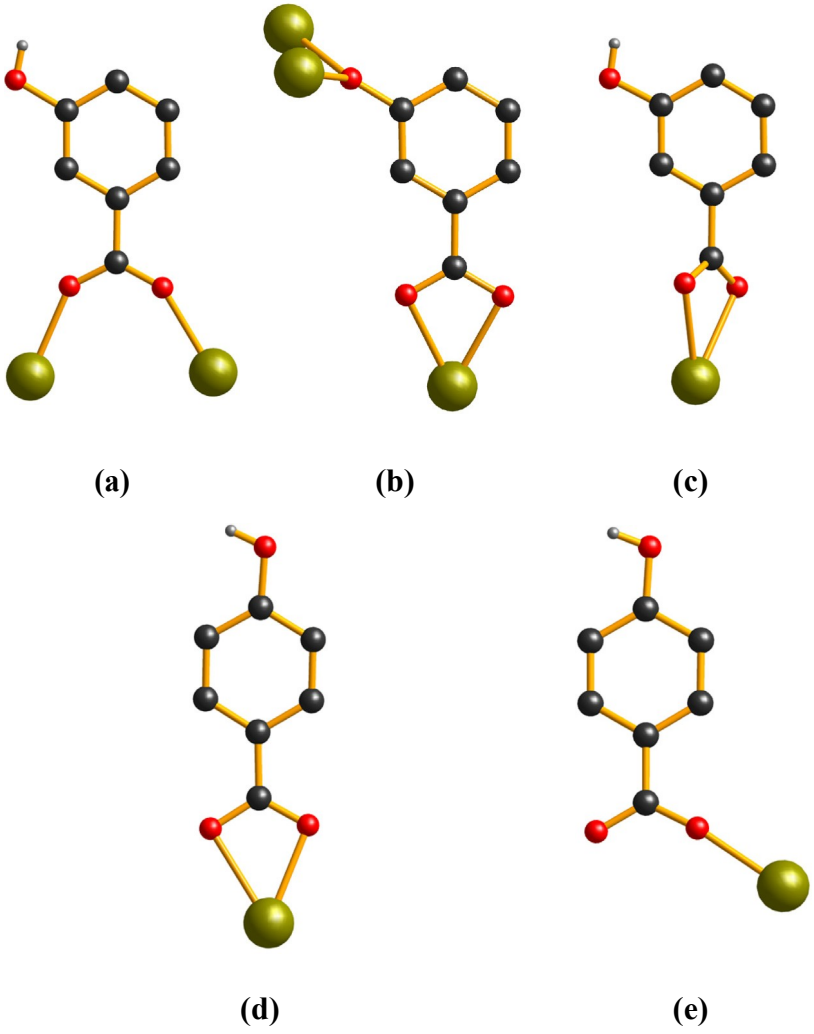

Scheme 1. Coordination modes for different forms of *m*-H_2L and *p*-H_2L ligands in 1–6.

interactions to form a 3-D supramolecular bct network. The asymmetric unit of 2 consists of one Gd(III) center, three *m*-HL ligands, and one chelating phen ligand. The Gd(III) ion is eight-coordinated and exhibits distorted square antiprismatic coordination geometry [16], which is surrounded by six oxygen atoms from five distinct *m*-HL ligands as well as two nitrogen atoms from one chelating phen ligand (Fig. 2a). For *m*-H_2L ligand in 2, only the carboxylate group is deprotonated to take the *m*-HL form. There are two different types of coordination modes for *m*-HL ligands in 2: *m*-HL-A links two Gd(III) ions by μ_2-η^1:η^1 bis-monodentate carboxylate group (Scheme 1a); *m*-HL-B coordinates to one Gd(III) ion through the μ_1-η^1:η^1 chelating carboxylate group (Scheme 1c). In 2, two adjacent Gd(III) ions are connected by four bridging *m*-HL ligands to afford a centrosymmetric dinuclear unit with the Gd···Gd distance of 4.3 Å. Significantly, a careful analysis of this structure indicates that the O6–H6A···O1^i hydrogen bonds (i = x, y + 1, z; see Table S3 for details) between hydroxyl group of *m*-HL-A and carboxylate oxygen of *m*-HL-B link the dinuclear units to generate a 1-D chain (Fig. 2b) [19]. The O3–H3B···O2^i hydrogen bonds (i = x−1, y −1/2, z + 1/2; see Table S3 for the details) between hydroxyl group and carboxylate oxygen of *m*-HL-A ligands further connect the adjacent 1-D chains to generate the 2-D layered net (Fig. 2b) [19]. If assuming the binuclear units as isolated nodes, the 2-D sheet can be regarded as a 2-D hxl (hexagonal lattice in 2-D net) layer (Fig. 2b) [17,22]. Furthermore, the 2-D sheets stack in the interdigitated fashion to generate a 3-D supramolecular array by π–π and C–H···π interactions (Fig. 2c). The face-to-face π···π interactions between the neighboring phenanthrolinic and the benzenic rings are characterized by the dihedral angle of 3.4° and the centroid···centroid distance of 3.7 Å, while those between the adjacent benzenic rings are characterized by the dihedral angle of 2.7° and the centroid···centroid distance of 3.7 Å (Table S2) [19]. The C–H···π interactions between the C30–H30A of phen ligand and adjacent phenanthrolinic rings (N1–C22–C23–C24–C25–C33) are characterized by the H···Cg separation of 2.84 Å and C–H···Cg angle of 148°, while the H···Cg separation and C–H···Cg angle of C17–H17A···Cg2 interactions between H17A from *m*-HL ligand and adjacent phenanthrolinic ring (N1–C22–C23–C24–C25–C33) are 2.93 Å and 146°, respectively (Table S2) [19]. To further briefly understand the structure of 2, each binuclear unit connects ten other ones and can be regarded as 10-connector. Hence, the overall structure of 2 is a 10-connected 3-D net, as shown in Fig. 2d. The Point (Schläfli) symbol for the net is ($3^{12}.4^{28}.5^5$) calculated by TOPOS program [20], which corresponds to a bct (body-centered tetragonal lattice net) topology [17,23].

3.2.3. Crystal structure of [Tb(m-HL)$_3$(phen)](3)

X-ray crystallographic study reveals that complex 3 crystallizes in space group $P2_1/c$ (see Table 1) and consists of neutral centrosymmetric dinuclear units, which are further connected by weak interactions to form a 3-D supramolecular hex network. The asymmetric unit of 3 contains one Tb(III) ion, one phen, and

three *m*-HL ligands. As shown in Fig. 3a, the central Tb(III) ion is eight-coordinated by six oxygen atoms from four distinct *m*-HL ligands as well as two nitrogen atoms from one chelating phen ligand to form a distorted square antiprismatic coordination sphere [16]. Similar to **2**, the two types of *m*-HL ligands are in bridging (*m*-HL-**A**, Scheme 1a) and chelating (*m*-HL-**B**, Scheme 1c) modes, respectively. Unlike **2**, the centrosymmetric dinuclear unit in **3** is made of two adjacent Tb(III) ions and only two bridging *m*-HL ligands with the Tb···Tb distance of 5.4 Å. The dinuclear units are further linked through O6–H6A···O7^{i} hydrogen bonds ($i = x, y+1, z$, H···O/O···O distance = 1.90/2.70 Å, angle = 164°) (Table S3) and C11–H11···p interactions (H···Cg separation: 3.00 Å; C–H···Cg angle: 99°) (Table S2) to form 1-D chain (Fig. S1) [19]. Then, the 2-D sheets are formed by the linkage of hydrogen bonds (O3–H3···O5^{i}: $i = x, -y+5/2, z-1/2$, H···O/O···O distance = 1.94/2.74 Å, angle = 163°), p···p (Cg, the centroid of the ring; Cg1: N1–C22–C23–C24–C25–C26; Cg2: C1–C2–C3–C4–C5–C6; Cg···Cg separation: 3.69 Å; dihedral angle: 14.6°), and C–H···p interactions (Cg3: C15–C16–C17–C18–C19–C20; H···Cg separation: 2.72 Å; C–H···Cg angle: 122°) (Tables S2, S3, and Fig. 3b) [19]. To simplify the 2-D network, each dinuclear unit can be regarded as isolated node and the 2-D network can be simplified as an **hxl** (hexagonal lattice in 2-D net) layer (Fig. 3b) [17,22]. Furthermore, the adjacent parallel 2-D sheets are linked by the O9–H9A···O3^{i} hydrogen-bonding interactions to form a 3-D supramolecular structure (Fig. 3c) ($i = x+2, y+2, z+2$; H···O/O···O distance = 1.96/2.78 Å, angle = 177°) (Table S3) [19]. From the topological view, each dinuclear unit connects to other eight ones and can be regarded as 8-connected node. Thus, the structure of **3** can be described as an 8-connected 3-D

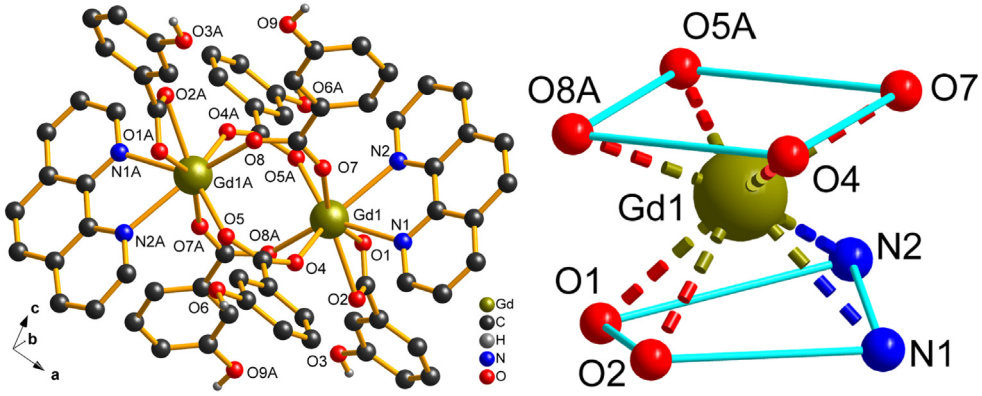

(a)

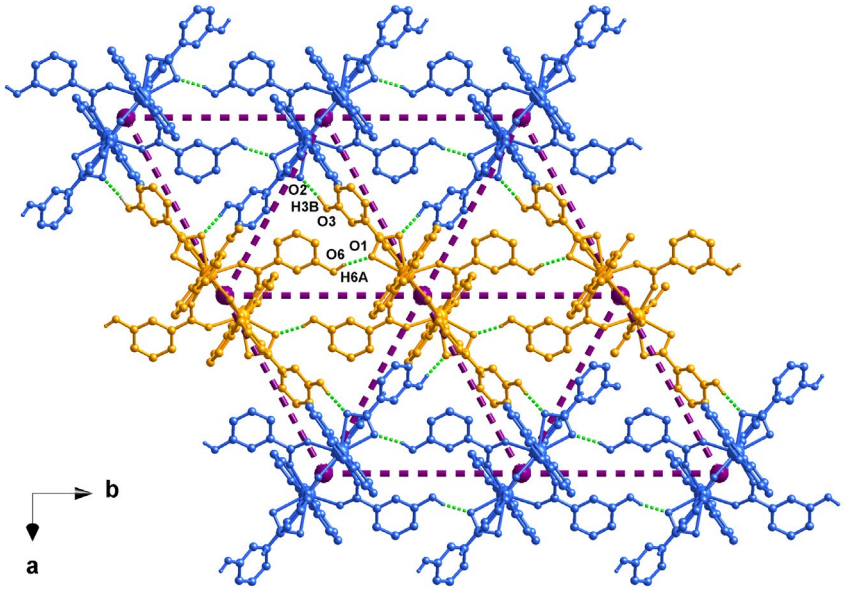

(b)

Fig. 2. (a) View of the local coordination environment (left) and coordination polyhedron (right) of Gd(III) ions in **2**. The atoms labeled with the suffix A is generated by the symmetry operation ($-x, -y+1, -z$). (b) View of the (3,6) 2-D **hxl** supramoleuclar network formed by O–H···O hydrogen-bonding interactions (green dashed lines) in **2** with the distinct 1-D chains shown in blue and orange colors. (c) View of the 3-D supramoleuclar framework formed by p···p and C–H···p interactions between adjacent layers with the different 2-D arrays are shown in blue and orange colors (left) and a local view of the p···p (pairs of p-rings are shown in the same colors) and C–H···p interactions (red dashed lines) (right). (d) Schematic view of the 3-D **bct** net, in which the intra- and inter-layer supramolecular interactions are depicted as purple and yellow dashed lines, respectively. (Color online.)

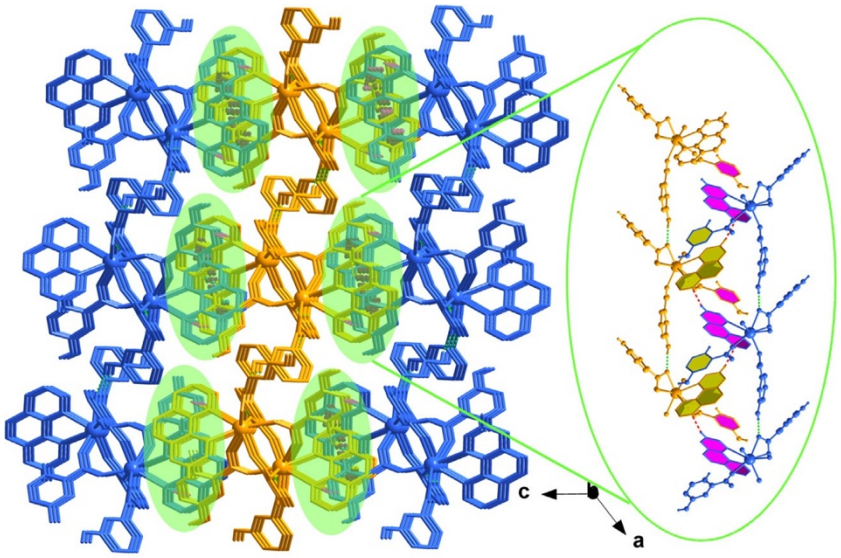

(c)

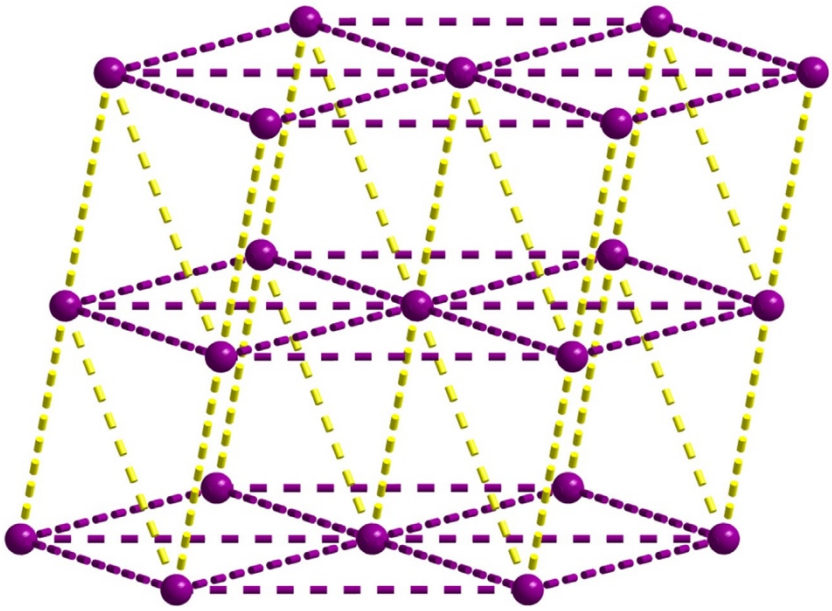

(d)

Fig. 2 (*continued*)

non-interpenetrating network with the Point (Schläfli) symbol ($3^6.4^{18}.5^3.6$) calculated by TOPOS program (Fig. 3d) [20], which corresponds to an hex (hexagonal lattice in 3-D net) topology [17,24].

3.2.4. Crystal structure of [Ln(p-HL)$_3$(phen)(H$_2$O)] (Ln = Dy for 4, Gd for 5, and Tb for 6)

The complexes 4–6 were obtained by the similar procedure for the preparation of 1–3 except using 4-hydroxybenzoic acid. The same space group and similar cell parameters (Table 1) indicate that complexes 4–6 are isostructural, so 4 is used for detailed structural description. The structure analysis shows that 4 consists of neutral centrosymmetric [Dy(*p*-HL)$_3$(phen)(H$_2$O)] mononuclear unit. There are one Dy(III) ion, three *p*-HL, one phen, and one coordinated water ligand in the asymmetric unit (Fig. 4a). The central Dy(III) ion is eight-coordinated by five oxygen atoms from three different *p*-HL ligands, one oxygen atom from coordinated water ligand, and two nitrogen atoms from phen ligand. The coordination geometry of the Dy(III) ion can be described as a distorted square antiprismoid (Fig. 4a) [16]. In 4, only the carboxylate group of *p*-H$_2$L is deprotonated to take the *p*-HL form. Each chelating (Scheme 1d) or monodentate (Scheme 1e) *p*-HL ligand links one Dy(III) ion. There are abundant hydrogen-bonding, p··· ·p and C–H···p interactions in 4. Firstly, the two adjacent mononuclear units are linked by O10–H1W···O4^i and O10–H2W···O6^i to form the dinuclear unit ($i = x-1, y, z$; see Table S3 for the details) [19]. Then, the O8–H8···O1^i hydrogen bonds link the dinuclear units to generate 1-D chain ($i = x, y+1, z$, see Table S3 for the details), in which the C–H···p interactions between H24A from phen ligand and adjacent benzene ring of *p*-HL are found (see

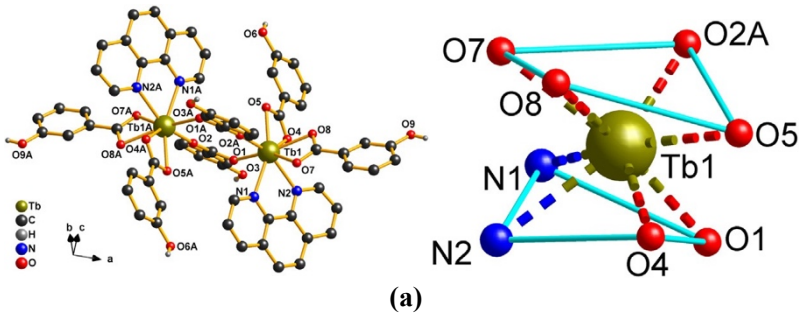

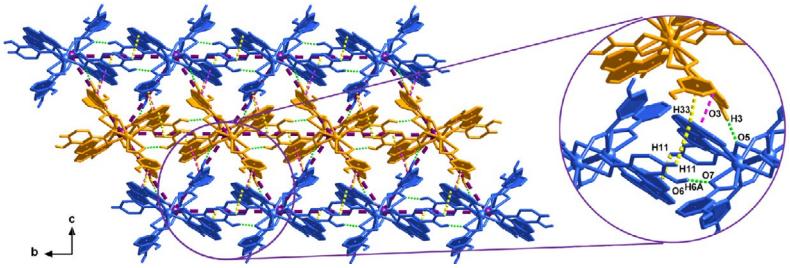

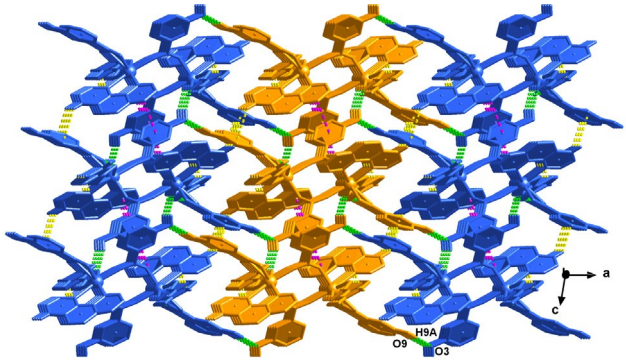

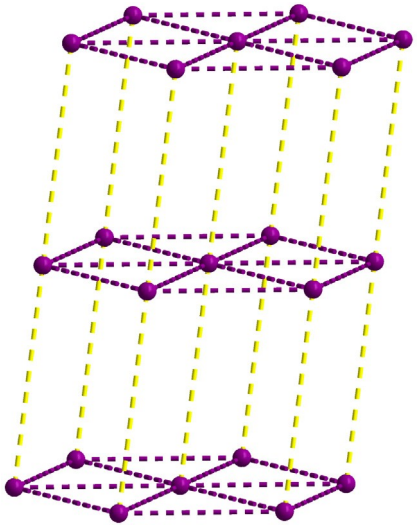

Fig. 3. (a) View of the local coordination environment (left) and coordination polyhedron (right) of Tb(III) ions in 3. The atoms labeled with the suffix A is generated by the symmetry operation (−*x* + 1, −*y* + 2, −*z* + 2). (b) (left) View of the (3,6) 2-D hxl supramoleuclar network formed by O–H··· ·O hydrogen-bonding (green dashed lines), p··· ·p (pink dashed lines), and C–H··· ·p (yellow dashed lines) interactions in 3 with the distinct 1-D chains shown in blue and orange colors. (right) The local view of the weak interactions in 3. (c) View of the 3-D supramoleuclar framework formed by O9–H9A··· ·O3 hydrogen-bonding interactions (green dashed lines) with the different 2-D arrays are shown in blue and orange colors. (d) Schematic view of the 3-D hex net. (Color online.)

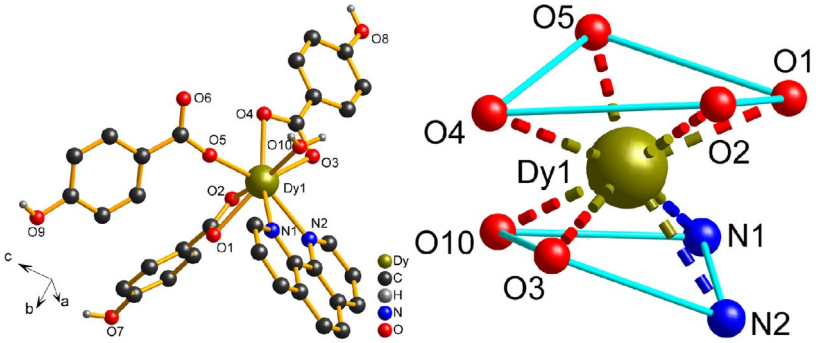

(a)

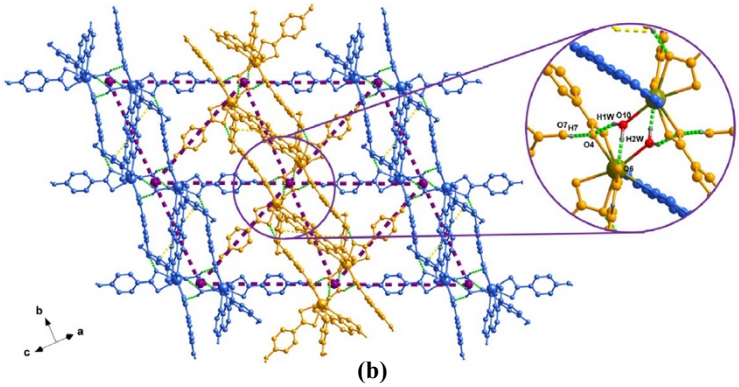

(b)

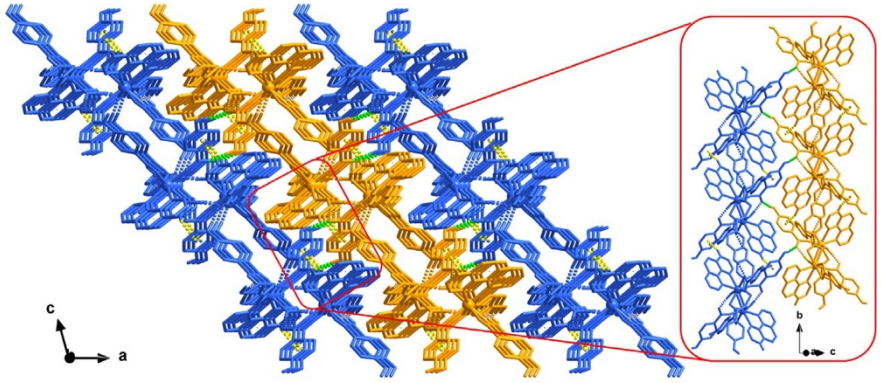

(c)

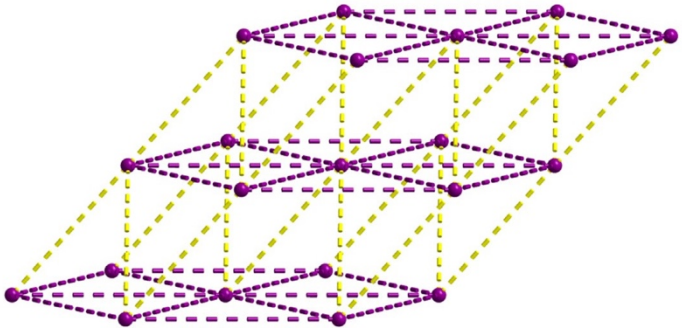

(d)

Fig. 4. (a) View of the local coordination environment (left) and coordination polyhedron (right) of Dy(III) ion in 4. (b) View of the (3,6) 2-D hxl supramoleuclar network formed by with the O–H··· ·O hydrogen-bonding (green dashed lines) and C–H··· ·p (yellow dashed lines) interactions (left) and a local view of the O–H··· ·O hydrogen-bonding interactions (right). (c) View of the 3-D framework formed by hydrogen bonds between adjacent layers with the different 2-D arrays are shown in blue and orange colors (left) and a local view of the hydrogen bonds (green dashed lines) (right). (d) Schematic view of the 3-D bct network, in which the intra- and inter-layer supramolecular interactions are depicted as purple and yellow dashed lines, respectively. (Color online.)

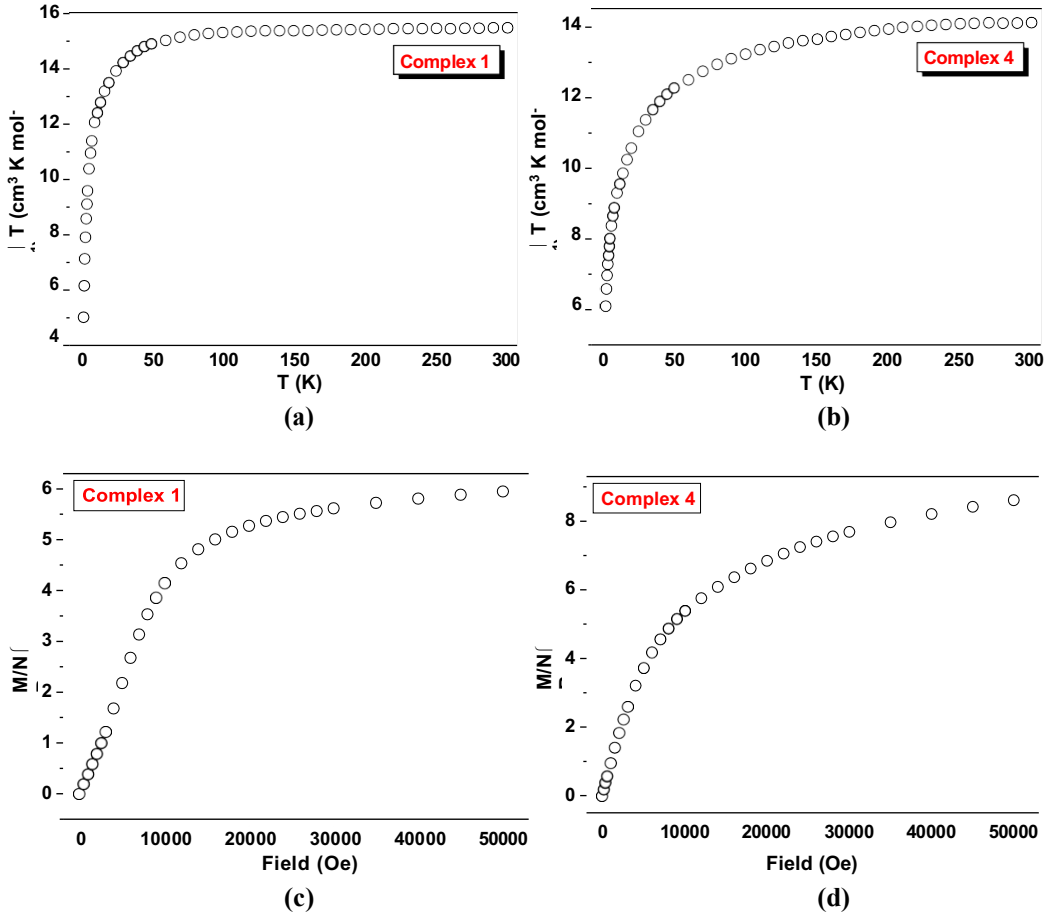

Fig. 5. *T* vs. *T* plots for 1 (a) and 4 (b) at an applied dc field of 1.0 T. Magnetization vs. field plots for 1 (c) and 4 (d) at 2 K.

Table S2 for the details) [19]. Furthermore, adjacent 1-D chains are connected by O7–H7 Ɵ4^{i} to generate the 2-D structure ($i = x$ – + 2, y + 1/2, = + 3/2, Table S3) (Fig. 4b) [19]. Finally, the 2-D motifs are further linked by hydrogen bonds to generate the 3-D structure (Fig. 4c). The O9–H9·O6^{i} hydrogen bonds involve in monodentate *p*-HL ligands (i = –x + 2, y + 1/2, = + 3/2, Table S3) [19]. To simplify the structure of 4, each dinuclear unit linked by O10–H1W·O4^{i} and O10–H2W··Ɵ6^{i} hydrogen bonds is treated as the isolated node. Each node connects to other eight ones via weak interactions to obtain an 8-connected 3-D network with the Point (Schläfli) symbol ($3^{12}.4^{28}.5^{5}$) calculated by TOPOS program (Fig. 3d) [20], which corresponds to a bct (body-centered tetragonal lattice net) topology [17,23].

3.3. Comparison of the structures for complexes 1–6

It is noteworthy that a variety of coordination structures can be achieved on the basis of the hydroxybenzoate isomers with differently oriented hydroxyl groups, lanthanoid(III) ions, and phen co-ligand. The phenomenon of supramolecular structural diversification in 1–6 may arise from the different coordination modes and positions of hydroxyl groups for organic ligands. Firstly, the hydroxybenzoate isomers exhibit several coordination patterns (Scheme 1). In 1, the *m*-H_2L ligands exhibit the *m*-HL and *m*-L forms. The carboxylate and hydroxyl groups are both deprotonated in the *m*-L form which connects three Dy(III) ions (Scheme 1b). Meanwhile, the *m*-H_2L or *p*-H_2L ligands in other complexes are partially deprotonated and only the carboxylate oxygen atoms coordinate to lanthanoid(III) ions (Scheme 1a, c, d and e). Because of the additional binding site from the hydroxyl group, complex 1 shows a 2-D coordination network while others are dinuclear or monomeric units. Secondly, the differently oriented hydroxyl groups in hydroxybenzoate isomers may play significant roles in the direction of formation of hydrogen bonds. In 1, the hydrogen bonds between the lattice water molecules and carboxylate/hydroxyl groups connect the 2-D layers to form 3-D supramolecular network. The hydrogen bonds between the hydroxyl and carboxylate groups link the dinuclear units to generate only 2-D layer in 2, while those link the dinuclear units to form the 3-D supramolecular framework in 3. For 4–6, the monomeric units firstly form the dimer through the hydrogen bonds around the coordinated water ligands. Then, the dimers were further connected by hydrogen bonds between the carboxylate and hydroxyl groups to obtain 3-D supramolecuar network.

3.4. Magnetic and photoluminescence properties of the complexes

To confirm whether the crystal structures are truly representative of the bulk materials, powder X-ray diffraction (PXRD) experiments have been carried out for complexes 1–6. The experimental and simulated PXRD patterns of the corresponding complexes are depicted in Fig. S2. Although the experimental patterns have a few unindexed diffraction lines and some peaks are slightly broadened in comparison with those simulated from the single crystal data, it still can be considered favorably that the bulk synthesized materials and the as-grown crystals are homogeneous for 1–6.

Magnetic susceptibility data for the crushed crystalline samples of complexes 1 and 4 were collected at an applied field of 1.0 T in

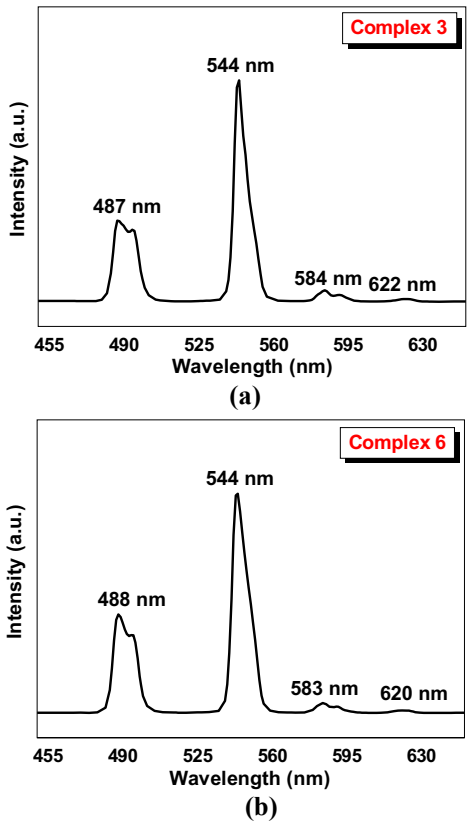

Fig. 6. Solid-state emission spectra of complexes 3 and 6 at room temperature: (a) for 3, (b) for 6.

2–300 K. As shown in Fig. 5a, the χT product of 1 has a value of 15.37 cm^3 K mol^{-1} at 300 K, slightly above the expected 14.2 cm^3 K mol^{-1} for one isolated Dy(III) ion ($^6H_{15/2}$, $S = 5/2$, $L = 5$, $J = 15/2$, $g_J = 4/3$). The χT product is nearly constant as the temperature decreases, until a sharp drop is observed below 50 K. The magnetization vs. field behavior of complex 1 at 2 K is shown in Fig. 5c. The saturation reaches at a value of 5.9 ▌B, below the expected for one Dy(III) ion due to the spin orbit coupling and anisotropy. The Dy (III) ion possesses usually strong spin–orbit coupling, and as usual for lanthanide ions, the coupling between metal centers is weak. Complex 1 is a 2-D network consisted of Dy_2 units. The Dy(III) ions in the Dy_2 units are linked by two monoatomic oxygen bridges from the hydroxyl groups of *m*-L ligands (Dy–O–Dy angle is 102.59°) and two *syn,syn*-carboxylate bridges. This should lead to a competition between weak ferromagnetic and weak antiferromagnetic coupling. The Dy_2 units are linked via a *meta* substituted aromatic ring, which should in turn provide an efficient pathway for weak ferromagnetic coupling [25]. Due to the structure of 1 it is not possible to model the magnetic data. The interactions in 1 are so weak that can only be observed in the lowest range of temperatures (below 4 K). As shown in Fig. 5b, The χT product of 4 has a value of 14.08 cm^3 K mol^{-1} at 300 K, as expected for one isolated Dy(III) ion ($^6H_{15/2}$, $S = 5/2$, $L = 5$, $J = 15/2$, $g_J = 4/3$). The χT product of 4 is nearly constant as temperature decreases, and below 100 K a drop is observed due to the depopulation of the excited stark sublevels. The magnetization vs. field behavior of complex 4 at 2 K is shown in Fig. 5d. The magnetization does not follow the Bril- louin law and not reaches the saturation even at 5 T applied dc field, due to the inherent spin–orbit coupling and anisotropy of Dy(III) ion.

The solid-state luminescent spectra of complexes 3 and 6 were investigated at room temperature (Fig. 6). The emission spectra of the free ligands *m*-H_2L, *p*-H_2L, phen are shown in Fig. S3. The free *m*-H_2L and *p*-H_2L ligands show the emission bands 346 nm (k_{ex} = 324 nm) and 424 nm (k_{ex} = 327 nm), whereas the phen ligand shows the fluorescent emission bands at 363, 382, 403 nm (k_{ex} = 345 nm). Under excitation at 354 nm, complexes 3 and 6 give typical Tb(III) emission spectra containing the expected sequence of $^5D_4$? ^7F_J ($J = 6$, 5, 4, 3) transitions, respectively, and the $^5D_4$? $^7F_5$ transition is the strongest emission (Fig. 6).

4. Conclusions

Through the self-assembly of *m*-/*p*-hydroxybenzoic acid isomers with phen and different rare earth oxides (Dy for 1 and 4, Gd for 2 and 5, and Tb for 3 and 6), two series of lanthanide supramolecular frameworks were obtained, respectively. Crystal structures as well as magnetic and luminescent properties of complexes 1–3 have also been investigated. The results reveal that the structural versatility of 1–3 and 4–6 can be tuned by the position isomers and coordination modes of hydroxybenzoic acid. This work expanded the research of the coordination possibilities related to the position isomers of hydroxybenzoic acid. Further work is in progress to prepare new coordination complexes based on the position isomers of hydroxybenzoic acid with novel topological networks and interesting chemical and physical properties.

Acknowledgements

We are grateful for the support from the National Natural Science Foundation of China (21471134 and 21571158) and Plan for Scientific Innovation Talent of Henan Province (154200510011). E.C.S. acknowledges the financial support from the Spanish Government (Grant CTQ2012-32247).

Appendix A. Supplementary data

CCDC 1456709-1456714 contain the supplementary crystallographic data for complexes 1–6, respectively. These data can be obtained free of charge via http://www.ccdc.cam.ac.uk/conts/retrieving.html, or from the Cambridge Crystallographic Data Centre, 12 Union Road, Cambridge CB2 1EZ, UK; fax: (+44) 1223-336-033; or e-mail: deposit@ccdc.cam.ac.uk. Supplementary data associated with this article can be found, in the online version, at http://dx.doi.org/10.1016/j.poly.2016.04.015.

References

[1] (a) Y. Tian, S. Shen, J. Cong, L. Yan, S. Wang, Y. Sun, J. Am. Chem. Soc. 138 (2016) 782;
(b) M. Chen, E.C. Sañudo, E. Jiménez, S.-M. Fang, C.-S. Liu, M. Du, Inorg. Chem. 53 (2014) 6708;
(c) R. Alam, K. Pal, B.K. Shaw, M. Dolai, N. Pal, S.K. Saha, M. Ali, Polyhedron 106 (2016) 84.
[2] (a) S.K. Elsaidi, M.H. Mohamed, T. Pham, T. Hussein, L. Wojtas, M.J. Zaworotko, B. Space, Cryst. Growth Des. 16 (2016) 1071;
(b) M. Du, C.-P. Li, M. Chen, Z.-W. Ge, X. Wang, L. Wang, C.-S. Liu, J. Am. Chem. Soc. 136 (2014) 10906;
(c) E. Coropceanu, A. Rija, V. Lozan, I. Bulhac, G. Duca, V.Ch. Kravtsov, P. Bourosh, Cryst. Growth Des. 16 (2016) 814.
[3] (a) G. Huang, L. Yang, X. Ma, J. Jiang, S.-H. Yu, H.-L. Jiang, Chem. Eur. J. 22 (2016) 3470;
(b) Z. Li, N.M. Schweitzer, A.B. League, V. Bernales, A.W. Peters, A. Getsoian, T. C. Wang, J.T. Miller, A. Vjunov, J.L. Fulton, J.A. Lercher, C.J. Cramer, L. Gagliardi, J. T. Hupp, O.K. Farha, J. Am. Chem. Soc. 138 (2016) 1977;
(c) L. Zhu, C.F. Tan, M. Gao, G.W. Ho, Adv. Mater. 27 (2015) 7713.
[4] (a) I. Kuzu, I. Krummenacher, I.J. Hewitt, Y. Lan, V. Mereacre, A.K. Powell, P. Höfer, J. Harmer, F. Breher, Chem. Eur. J. 15 (2009) 4350;
(b) A. Mahmood, R. Zou, Q. Wang, W. Xia, H. Tabassum, B. Qiu, R. Zhao, ACS Appl. Mater. Interfaces 8 (2016) 2148;
(c) L. Tabrizi, H. Chiniforoshan, P. McArdle, H. Tavakol, B. Rezaei, M.M. Dehcheshmeh, Polyhedron 69 (2014) 84.

[5] (a) Z.-F. Wu, B. Tan, Z.-H. Deng, Z.-L. Xie, J.-J. Fu, N.-N. Shen, X.-Y. Huang, Chem. Eur. J. 22 (2016) 1334;
(b) Y. Yu, J.-P. Ma, C.-W. Zhao, J. Yang, X.-M. Zhang, Q.-K. Liu, Y.-B. Dong, Inorg. Chem. 54 (2015) 11590.
[6] A.Y. Robin, K.M. Fromm, Coord. Chem. Rev. 250 (2006) 2127.
[7] (a) J. Yang, L. Zhou, J. Cheng, Z. Hu, C. Kuo, C.-W. Pao, L. Jang, J.-F. Lee, J. Dai, S. Zhang, S. Feng, P. Kong, Z. Yuan, J. Yuan, Y. Uwatoko, T. Liu, C. Jin, Y. Long, Inorg. Chem. 54 (2015) 6433;
(b) C. Hua, P. Turner, D.M. D'Alessandro, Dalton Trans. 44 (2015) 15297.
[8] (a) R. Wang, X. Liu, A. Huang, W. Wang, Z. Xiao, L. Zhang, F. Dai, D.-F. Sun, Inorg. Chem. 55 (2016) 1782;
(b) J. Cai, J. Yu, H. Wang, X. Duan, Q. Zhang, C. Wu, Y. Cui, Y. Yu, Z. Wang, B. Chen, G. Qian, Cryst. Growth Des. 15 (2015) 4071.
[9] (a) C. Wang, L. Li, S. Tang, X. Zhao, ACS Appl. Mater. Interfaces 6 (2014) 16932;
(b) Y. Cui, R. Song, J. Yu, M. Liu, Z. Wang, C. Wu, Y. Yang, Z. Wang, B. Chen, G. Qian, Adv. Mater. 27 (2015) 1420.
[10] (a) M. Chen, H. Zhao, C.-S. Liu, X. Wang, H.-Z. Shi, M. Du, Chem. Commun. 51 (2015) 6014;
(b) Z.-W. Wang, M. Chen, C.-S. Liu, X. Wang, H. Zhao, M. Du, Chem. Eur. J.21 (2015) 17215.
[11] (a) H. Deng, S. Grunder, K.E. Cordova, C. Valente, H. Furukawa, M. Hmadeh, F. Gándara, A.C. Whalley, Z. Liu, S. Asahina, H. Kazumori, M. O'Keeffe, O. Terasaki, J.F. Stoddart, O.M. Yaghi, Science 336 (2012) 1018;
(b) M. Eddaoudi, J. Kim, N. Rosi, D. Vodak, J. Wachter, M. O'Keeffe, O.M. Yaghi, Science 295 (2002) 469.
[12] (a) J.H. Park, W.R. Lee, D.W. Ryu, K.S. Lim, E.A. Jeong, W.J. Phang, E.K. Koh, C.S. Hong, Cryst. Growth Des. 12 (2012) 2691;
(b) F.-P. Huang, J.-L. Tian, G.-J. Chen, D.-D. Li, W. Gu, X. Liu, S.-P. Yan, D.-Z. Liao, P. Cheng, CrystEngComm 12 (2010) 1269.
[13] C.-S. Liu, M. Du, E.C. Sañudo, J. Echeverria, M. Hu, Q. Zhang, L.-M. Zhou, S.-M. Fang, Dalton Trans. 40 (2011) 9366.
[14] CrysAlis CCD and CrysAlis RED, version 1.171.33.55, Oxford Diffraction Ltd., Yarnton, Oxfordshire, U.K., 2010.
[15] (a) G.M. Sheldrick, SHELXTL, version 6.10, Bruker Analytical X-ray Systems, Madison, WI, 2001;
(b) G.M. Sheldrick, Acta Crystallogr. A 64 (2008) 112.
[16] S. Mishra, E. Jeanneau, H. Chermette, S. Daniele, L.G. Hubert-Pfalzgraf, Dalton Trans. (2008) 620.
[17] O'Keeffe, M. see website: http://rcsr.net.
[18] (a) P. Metrangolo, F. Meyer, T. Pilati, D.M. Proserpio, G. Resnati, Chem. Eur. J. 13 (2007) 5765;
(b) Q. Fang, G. Zhu, M. Xue, Z. Wang, J. Sun, S. Qiu, Cryst. Growth Des. 8 (2008) 319.
[19] A.L. Spek, J. Appl. Crystallogr. 36 (2003) 7.
[20] V.A. Blatov, TOPOS, A Multipurpose Crystallochemical Analysis with the Program Package; Samara State University, Russia, 2004.
[21] (a) T.-T. Luo, H.-L. Tsai, S.-L. Yang, Y.-H. Liu, R.D. Yadav, C.-C. Su, C.-H. Ueng, L.-G. Lin, K.-L. Lu, Angew. Chem., Int. Ed. 44 (2005) 6063;
(b) Q.-R. Fang, G.-S. Zhu, Z. Jin, M. Xue, X. Wei, D.-J. Wang, S.-L. Qiu, Angew. Chem., Int. Ed. 45 (2006) 6126.
[22] (a) J. Jia, A.J. Blake, N.R. Champness, P. Hubberstey, C. Wilson, M. Schröder, Inorg. Chem. 47 (2008) 8652;
(b) Z. Pan, J. Xu, H. Zheng, K. Huang, Y. Li, Z. Guo, S.R. Batten, Inorg. Chem. 48 (2009) 5772.
[23] (a) F.-N. Shi, L. Cunha-Silva, T. Trindade, F.A.A. Paz, J. Rocha, Cryst. Growth Des. 9 (2009) 2098;
(b) Z. Su, Y. Song, Z.-S. Bai, J. Fan, G.-X. Liu, W.-Y. Sun, CrystEngComm 12 (2010) 4339.
[24] (a) N.L. Rosi, J. Kim, M. Eddaoudi, B. Chen, M. O'Keeffe, O.M. Yaghi, J. Am. Chem. Soc. 127 (2005) 1504;
(b) X.-F. Wang, Y.-B. Zhang, X.-N. Cheng, X.-M. Chen, CrystEngComm 10 (2008) 753.
[25] (a) S.-M. Fang, E.C. Sañudo, M. Hu, Q. Zhang, S.-T. Ma, L.-R. Jia, C. Wang, J.-Y. Tang, M. Du, C.-S. Liu, Cryst. Growth Des. 11 (2011) 811;
(b) R.H. Lay, E.C. Sañudo, Inorg. Chim. Acta 362 (2009) 2205;
(c) A.R. Paital, T. Mitra, D. Ray, W.T. Wong, J. Ribas-Ariño, J.J. Novoa, J. Ribas, G. Aromi, Chem. Commun. (2005) 5172.